Constitutive Equations for Anisotropic Continua

J.A. Goshawk and R.S. Jones
Department of Mathematics
University of Wales Aberystwyth
Penglais, Aberystwyth
Ceredigion, SY23 3BZ

Abstract

Two classes of simple constitutive equations for continuous fibre-reinforced composites are introduced. In the first, the transverse and longitudinal viscosities are functions of invariants of the rate-of-strain tensor and the fibre-orientation vector. In the second, anisotropic yield conditions are imposed. The response of each of the models in a stratified flow is considered.

1 Introduction

To model the flow of materials it is necessary to derive appropriate constitutive descriptions for the materials concerned. In the case of anisotropic materials there are a number of stress–strain and stress–rate-of-strain relationships which enable a range of materials possessing directional properties to be modelled. In this present study the materials of primary concern are continuous fibre-reinforced composites (CFRCs) which are transversely isotropic. An account of the theory of transversely isotropic materials is given in Hull et al. [1] where a number of models are described. In particular they derive the anisotropic counterpart of the isotropic Reiner–Rivlin fluid for ideal fibre-reinforced fluids that are both inextensible in the fibre direction and incompressible. A special case of this is the linear form with constant viscosities

$$\sigma_{ij} = -p\delta_{ij} + Ta_ia_j + 2\eta_T d_{ij} + 2\left(\eta_L - \eta_T\right)\left(a_ia_kd_{kj} + a_ja_kd_{ik}\right). \qquad (1)$$

where σ_{ij}, δ_{ij}, d_{ij} and a_i are the Cartesian components of the stress tensor, identity tensor, rate-of-strain tensor and the fibre-orientation vector respectively. The constant longitudinal and transverse viscosities are η_L and η_T respectively, the isotropic pressure is denoted p and the tension T is a tension is a reaction force arising from the inextensibility constraint

$$a_i a_j \frac{\partial v_i}{\partial x_j} = 0, \tag{2}$$

where v_i are the components of the velocity vector. This constraint is implied in the convected equations

$$\frac{\partial a_i}{\partial t} + v_j \frac{\partial a_i}{\partial x_j} = a_j \frac{\partial v_i}{\partial x_j}. \tag{3}$$

Some experimental studies on CFRCs have found these materials to possess a variable viscosity and/or a yield stress. It is therefore of interest to consider anisotropic models that mimic these qualities.

2 Anisotropic models with variable viscosity functions

A model that is commonly used to describe isotropic materials with a variable viscosity is the generalized Newtonian model

$$\sigma_{ij} = -p\delta_{ij} + 2\eta\left(II^{\frac{1}{2}}\right) d_{ij}, \tag{4}$$

in which the viscosity η is a function of $II = 2d_{ij}d_{ij}$, the second rate-of-strain invariant. As an anisotropic counterpart to the generalized Newtonian model we generalize eq. (1) by assuming that η_L and η_T are functions of the two independent invariants

$$I_1^2 = 2d_{ij}d_{ij}, \qquad I_2^2 = 4a_i d_{ij} d_{jk} a_k. \tag{5}$$

Two functional forms for η_L and η_T are considered based on the isotropic Cross model [2] which has proved effective in characterizing isotropic materials with shear-rate dependent viscosities. In the first it is assumed that both η_L and η_T depend on the invariant I_1 only, so that

$$\eta_s = \eta_s^\infty + \frac{\eta_s^0 - \eta_s^\infty}{1 + (C_s\,|I_1|)^{1-n_s}}, \qquad s = L, T. \tag{6}$$

In the second, in order to reflect directional differences in the viscous response

$$\eta_L = \eta_L^\infty + \frac{\eta_L^0 - \eta_L^\infty}{1 + (C_L\,|I_2|)^{1-n_L}}, \qquad \eta_T = \eta_T^\infty + \frac{\eta_T^0 - \eta_T^\infty}{1 + (C_T\,|J|)^{1-n_T}}, \tag{7}$$

where $J^2 = I_1^2 - I_2^2$. In the above expressions for η_L and η_T the model parameters are defined as follows: n_s are power-law exponents, η_s^∞ and η_s^0 refer to asymptotic values of the viscosity at very high and very low shear rates respectively and C_s are constant parameters with the dimension of time. In all the viscosity models if $n_s = 1$ the viscosity becomes constant and eq. (1) is recovered. Additionally, if $n_s > 1$ the viscosity increases with value of the invariant and conversely if $n_s < 1$ it decreases.

3 An anisotropic yield stress model

In this section, characteristics of an isotropic yield stress model are combined with the anisotropic model given in eq. (1) to produce an anisotropic yield stress model. A frequently used isotropic yield stress model is that due to Bingham [3] and in 1947 Oldroyd [4] provided a properly invariant formulation of the Bingham fluid which can be written

$$\sigma_{kk} = 3\kappa\Delta, \tag{8}$$

$$\sigma_{ij} = -p\delta_{ij} + \sigma'_{ij}, \tag{9}$$

$$\sigma'_{ij} = 2\mu\epsilon_{ij}, \qquad \left(\tfrac{1}{2}\sigma'_{ij}\sigma'_{ij} \le \sigma_y^2\right), \tag{10}$$

$$\sigma'_{ij} = 2\left(\eta_1 + \sigma_y\left(2d_{kl}d_{kl}\right)^{-\frac{1}{2}}\right)d_{ij}, \qquad \left(\tfrac{1}{2}\sigma'_{ij}\sigma'_{ij} \ge \sigma_y^2\right). \tag{11}$$

The quantity Δ is the dilation of the material and σ'_{ij} and ϵ_{ij} are components of the extra stress and strain tensors. The rigidity and bulk moduli are given by μ and κ respectively, while η_1 and σ_y denote the reciprocal mobility and the value at which the material yields. All other quantities are as previously defined.

A natural extension of the model given by eqs. (8–11) to an anisotropic model is

$$\sigma_{kk} = 3\kappa\Delta, \tag{12}$$

$$\sigma_{ij} = -p\delta_{ij} + Ta_ia_j + \sigma'_{ij}, \tag{13}$$

$$\sigma'_{ij} = 2\mu\epsilon_{ij}, \qquad \left(\tfrac{1}{2}\sigma'_{ij}\sigma'_{ij} \le \tfrac{1}{2}f_{ij}f_{ij}\right), \tag{14}$$

$$\sigma'_{ij} = 2\eta_T d_{ij} + 2\left(\eta_L - \eta_T\right)\left(a_ia_kd_{kj} + a_ja_kd_{ik}\right) + f_{ij}, \qquad \left(\tfrac{1}{2}\sigma'_{ij}\sigma'_{ij} \ge \tfrac{1}{2}f_{ij}f_{ij}\right), \tag{15}$$

where f_{ij} are components of the yield stress tensor given by

$$f_{ij} = \frac{1}{(2d_{kl}d_{kl})^{\frac{1}{2}}} \left(2\sigma_T d_{ij} + 2\left(\sigma_L - \sigma_T\right)\left(a_i a_k d_{kj} + a_j a_k d_{ik}\right)\right), \qquad (16)$$

in which σ_T and σ_L are the yield stresses transverse and perpendicular to the fibre directions respectively. The model predicts that below the yield value the material behaves like an isotopic elastic solid and upon yielding the directional properties of the material are important and it behaves as an anisotropic liquid. The yield condition itself is anisotropic having different values depending upon the direction of the fibres.

For isotropic yield stress models it is commonly assumed that the material is inelastic prior to yielding [5]. If this is the case then $\mu \to \infty$ and eq. (14) is replaced by

$$d_{ij} = 0, \qquad \left(\tfrac{1}{2}\sigma'_{ij}\sigma'_{ij} \leq \tfrac{1}{2}f_{ij}f_{ij}\right). \qquad (17)$$

It has been pointed out [6], that using eq. (17) can cause problems with numerical schemes since numerical noise will always produce non-zero values for d_{ij}. In addition, it is not possible to determine the stresses in the unyielded region. One solution to these problems is to assume that the material behaves like an extremely viscous Newtonian fluid below the yield stress, that is

$$\sigma'_{ij} = 2\eta_y d_{ij}, \qquad \left(\tfrac{1}{2}\sigma'_{ij}\sigma'_{ij} \leq \tfrac{1}{2}f_{ij}f_{ij}\right), \qquad (18)$$

where the Newtonian viscosity $\eta_y \gg \eta_L$ and η_T. Using eq. (18) means that the material flows (albeit very slightly) isotropically below the yield condition. This ploy has the disadvantage that there will be a discontinuity of stress on yielding. It is also possible to build in anisotropic deformation in the 'unyielded' region but due to the fact that the deformation is negligible at stresses below the yield vaule this appears to be an unnecessary complication.

4 Steady flow

The response of the models proposed in this paper in steady flow is now examined.

Recently, Goshawk and Jones [7] considered the flow of continuous fibre-reinforced composites in a steady flow. The model laminate was comprised of distinct resin layers and plies stacked alternately. In the current work a similar arrangement is used; however the resin layers and plies need not alternate in the stack thus two or more plies (or resin layers) may be placed adjacent to each other. This new arrangement further generalizes the model

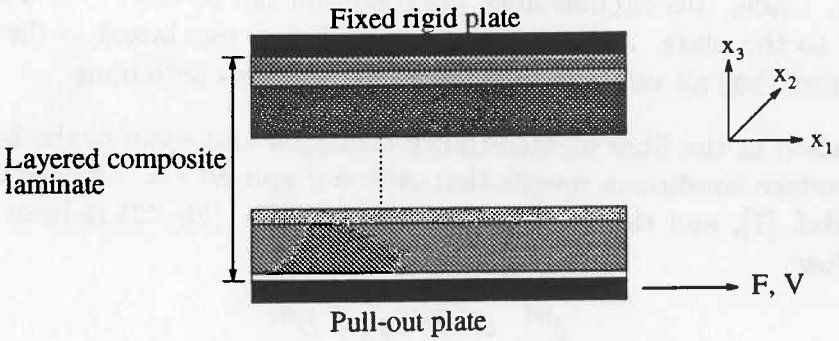

Figure 1: Geometrical set-up and orientation

of the laminate. The analysis follows closely the aforementioned work of Goshawk and Jones [7] for the shear flow of anisotropic materials with constant viscosity functions.

The problem is referred to a Cartesian frame of reference $O(x_1, x_2, x_3)$, arranged as shown in Fig. 1. The layered composite laminate is sandwiched between two rigid plate, one of which is fixed while a given force F or velocity V is applied to the other. It is assumed that the flow is sufficiently slow for inertial terms in the equations of motion to be neglected. Additionally, any body forces are assumed to be far lower than viscous forces and the equations of motion reduce to

$$\frac{\partial \sigma_{ij}}{\partial x_j} = 0. \tag{19}$$

The material is incompressible so the equation of continuity is $d_{ii} = 0$. Following Goshawk and Jones [7], the velocity distribution is assumed to be

$$v_1^{(r)} = A^{(r)}x_1 + B^{(r)}x_2 + C^{(r)}x_3 + D^{(r)}, \tag{20}$$

$$v_2^{(r)} = E^{(r)}x_1 - A^{(r)}x_2 + F^{(r)}x_3 + G^{(r)}, \tag{21}$$

$$v_3^{(r)} = 0, \tag{22}$$

which gives shear, extensional and translational components to the flow and satisfies the continuity equation exactly. The fibre direction in each layer is taken to be

$$\mathbf{a} = \left(\cos\alpha^{(r)}, \sin\alpha^{(r)}, 0\right). \tag{23}$$

The boundary conditions are applied at the interfaces of the laminate and the rigid plates at which it is assumed there is no slip. Additionally, the applied force on the pull-out plate is equal to the resultant shear traction imposed by the resin on that plate. This condition is not required to determine the velocity distribution through the laminate if the velocity of the pull-out plate

is given. Under this circumstance the condition can be used to find the force applied to the plate. At an interface between any two layers in the stack it is assumed that all velocities and shear stresses are continuous.

Application of the fibre inextensibility condition and some of the boundary and interface conditions reveals that $A^{(r)} = 0$ and $B^{(r)} = -E^{(r)} = 0$, for all r, see Ref. [7], and the velocity field given in eqs. (20–22) reduces to pure shear flow

$$v_1^{(r)} = C^{(r)}x_3 + D^{(r)}, \tag{24}$$
$$v_2^{(r)} = F^{(r)}x_3 + G^{(r)}, \tag{25}$$
$$v_3^{(r)} = 0. \tag{26}$$

The velocity field has been reduced to eqs. (24–26) using arguments related to the kinematics of the flow and the inextensibility of the fibres and to proceed further the stress distributions in the resin layers and plies are required.

4.1 Stress distributions

4.1.1 Resin layers

The constitutive equations to be used for the plies have been outlined in sections 2 and 3, however no attention has been paid to the constitutive description of the resin layers. It is quite plausible for the resin layers to follow the isotopic equivalent stress–rate-of-strain relation to the anisotropic relation used for the plies. However, for the sake of simplicity it is assumed that all resin layers are Newtonian in nature and as such the constitutive equation is the familiar

$$\sigma_{ij} = -p\delta_{ij} + \eta d_{ij}. \tag{27}$$

Consequently, it is straightforward to show that if the r^{th} layer is a resin layer then the stress distribution is that layer, generated by the velocity field in eqs. (24–26), is

$$\begin{aligned} &\sigma_{11}^{(r)} = \sigma_{22}^{(r)} = \sigma_{33}^{(r)} = -p^{(r)}, \\ &\sigma_{12}^{(r)} = 0, \\ &\sigma_{13}^{(r)} = \eta^{(r)}C^{(r)}, \qquad \sigma_{23} = \eta^{(r)}F^{(r)}. \end{aligned} \tag{28}$$

4.1.2 Plies — variable viscosity model

If it is assumed that the r^{th} layer in the laminate is a ply that follows a stress–rate-of-strain relationship given in eq. (1) with η_L and η_T given by either eq. (6) or eq. (7), then on applying the velocity field given in eqs. (24–26) in conjunction with the fibre-orientation vector the following stress field is produced in the ply.

$$\begin{aligned}
\sigma_{11}^{(r)} &= -p^{(r)} + T^{(r)} \cos^2 \alpha^{(r)}, \\
\sigma_{22}^{(r)} &= -p^{(r)} + T^{(r)} \sin^2 \alpha^{(r)}, \\
\sigma_{33}^{(r)} &= -p^{(r)}, \\
\sigma_{12}^{(r)} &= T^{(r)} \cos^2 \alpha^{(r)} \sin^2 \alpha^{(r)}, \\
\sigma_{13} &= C^{(r)} \eta_T \\
&\quad + (\eta_L - \eta_T) \left(C^{(r)} \cos^2 \alpha^{(r)} + F^{(r)} \cos \alpha^{(r)} \sin \alpha^{(r)} \right), \\
\sigma_{23} &= F^{(r)} \eta_T \\
&\quad + (\eta_L - \eta_T) \left(F^{(r)} \sin^2 \alpha^{(r)} + C^{(r)} \cos \alpha^{(r)} \sin \alpha^{(r)} \right),
\end{aligned} \tag{29}$$

where η_L and η_T depend upon the invariants I_1, I_2 and J through eqs. (6) and (7) and

$$I_1 = \left(C^{(r)2} + F^{(r)2} \right)^{\frac{1}{2}}, \tag{30}$$

$$I_2 = C^{(r)} \cos \alpha + F^{(r)} \sin \alpha, \tag{31}$$

$$J = C^{(r)} \sin \alpha - F^{(r)} \cos \alpha. \tag{32}$$

4.1.3 Plies — yield stress model

On applying the shear flow velocity distribution, eqs. (24–26), together with the fibre-orientation vector, eq. (23), to a ply which is the r^{th} layer in the stack, and follows a constitutive relation given by eqs. (12–15), produces the following stress distribution;

$$\begin{aligned}
\sigma_{11}^{(r)} &= -p^{(r)} + T^{(r)} \cos^2 \alpha^{(r)}, \\
\sigma_{22}^{(r)} &= -p^{(r)} + T^{(r)} \sin^2 \alpha^{(r)}, \\
\sigma_{33}^{(r)} &= -p^{(r)}, \\
\sigma_{12}^{(r)} &= T^{(r)} \cos^2 \alpha^{(r)} \sin^2 \alpha^{(r)},
\end{aligned}$$

$$\sigma_{13}^{(r)} = \begin{cases} \eta_y^{(r)} C^{(r)}, & \left(\frac{1}{2}\sigma'_{ij}\sigma'_{ij} \le \frac{1}{2}f_{ij}f_{ij}\right) \\ \eta_T^{(r)} C^{(r)} + \left(\eta_L^{(r)} - \eta_T^{(r)}\right)\left(C^{(r)}\cos^2\alpha^{(r)} + F^{(r)}\cos\alpha^{(r)}\sin\alpha^{(r)}\right) & \\ + \left(\sigma_T^{(r)} C^{(r)} + \left(\sigma_L^{(r)} - \sigma_T^{(r)}\right)\left(C^{(r)}\cos^2\alpha^{(r)}\right.\right. & \\ \left.\left. + F^{(r)}\cos\alpha^{(r)}\sin\alpha^{(r)}\right)\right) \Big/ \left(C^{(r)2} + F^{(r)2}\right)^{\frac{1}{2}} & \\ & \left(\frac{1}{2}\sigma'_{ij}\sigma'_{ij} \ge \frac{1}{2}f_{ij}f_{ij}\right) \end{cases}$$

$$\sigma_{23}^{(r)} = \begin{cases} \eta_y^{(r)} F^{(r)}, & \left(\frac{1}{2}\sigma'_{ij}\sigma'_{ij} \le \frac{1}{2}f_{ij}f_{ij}\right) \\ \eta_T^{(r)} F^{(r)} + \left(\eta_L^{(r)} - \eta_T^{(r)}\right)\left(F^{(r)}\sin^2\alpha^{(r)} + C^{(r)}\cos\alpha^{(r)}\sin\alpha^{(r)}\right) & \\ + \left(\sigma_T^{(r)} F^{(r)} + \left(\sigma_L^{(r)} - \sigma_T^{(r)}\right)\left(F^{(r)}\sin^2\alpha^{(r)}\right.\right. & \\ \left.\left. + C^{(r)}\cos\alpha^{(r)}\sin\alpha^{(r)}\right)\right) \Big/ \left(C^{(r)2} + F^{(r)2}\right)^{\frac{1}{2}} & \\ & \left(\frac{1}{2}\sigma'_{ij}\sigma'_{ij} \ge \frac{1}{2}f_{ij}f_{ij}\right) \end{cases} \tag{33}$$

where

$$\tfrac{1}{2}f_{ij}f_{ij} = \sigma_T^{(r)2} + \frac{\sigma_L^{(r)2} - \sigma_T^{(r)2}}{C^{(r)2} + F^{(r)2}}\left(C^{(r)}\cos\alpha^{(r)} + F^{(r)}\sin\alpha^{(r)}\right)^2. \tag{34}$$

4.2 Preliminary results

It should be noted that the stress distributions given in eqs. (28), (29) and (33) do not depend on the coordinate axes x_1, x_2, x_3 and thereby satisfy the equations of motion, given in (19), identically. The values of $C^{(r)}$ and $F^{(r)}$ in each of the layers in the stack can be found by using the remaining boundary and interface conditions. Due to the non-linear nature of the equations for the plies, it is not possible to write down analytic expressions for $C^{(r)}$ and $F^{(r)}$ similar to those obtained by Goshawk and Jones [7]. Solutions are obtainable using numerical techniques and some preliminary results are presented here.

The initial geometrical configuration considered for the variable viscosity model is shown in Fig. 2. In this simplified example the laminate consists of two resin layers, each adjacent to one of the rigid plates, and one ply sandwiched between the resin layers. In all, eight cases have been examined; four combinations of the values of n_L and n_T have been used in both formulations of η_L and η_T given in eqs. (6) and (7). The values of the parameters used are given in Appendix A.

A velocity of 5 mm/s is applied to the lower rigid plate in the x_1-direction.

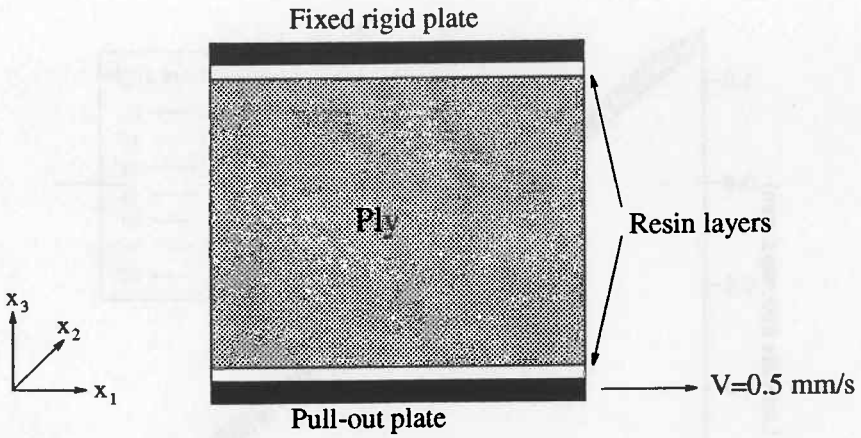

Figure 2: Geometrical configuration for the variable viscosity model example

Since a velocity is applied, instead of a force, the velocity fields generated for all of the cases considered are very similar. Typical examples of the velocity fields in the x_1 and x_2-directions are shown in Figs. 3 and 4 respectively. In Fig. 3 as the fibres are rotated from 0 to 90^o it becomes harder to shear the ply due to the fact that for the parameters chosen η_L is always less than η_T. The velocity in the x_2-direction, shown in Fig. 4, is zero if the fibres are at 0 or 90^o to the x_1-direction. For any other fibre angles a velocity field is generated in which there in flow in both the positive and negative x_2-directions within the ply. Such a velocity field has been shown to be a characteristic feature of the flow anisotropic materials in steady shear [7].

Fig. 5 shows the shear stress in the pull-out direction, σ_{13} as a function of fibre angle in each of the four cases, for both formulations of η_L and η_T. It is evident that the stresses are practically the same which implies that on measuring σ_{13}, generated in an experiment, insufficient information would be gained to determine which of the models to employ in a simulation. The shear stress perpendicular to the pull-out direction, σ_{23}, though, shown in Fig. 6, is symmetric about 45^o for the viscosity functions involving I_1 and not symmetric about 45^o for the viscosity functions involving I_2 and J. Hence, if σ_{23} is found to differ in two tests carried out at fibre orientations of α and $90-\alpha$ then viscosity functions involving I_2 and J should be employed in any simulation.

The viscosity functions, η_L and η_T, behave very differently for the two formulations as the fibre angle is varied. In Figs. 7 and 8 the viscosity functions are plotted for case 1 and the contrasting behaviour is clear. Similar behaviour is observed in the other three cases.

For the anisotropic yield stress material, the flow in a laminate consisting

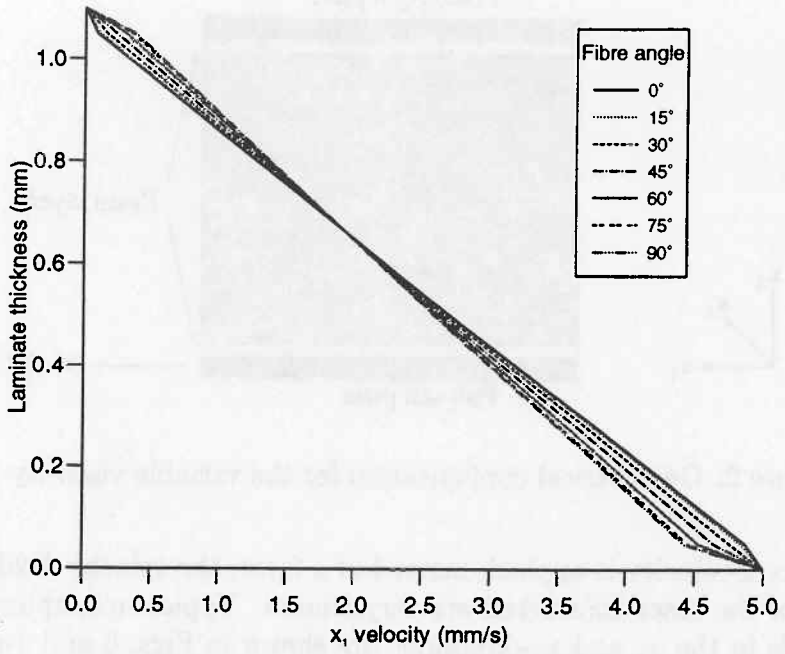

Figure 3: Variable viscosity model: typical velocity distribution in the x_1-direction

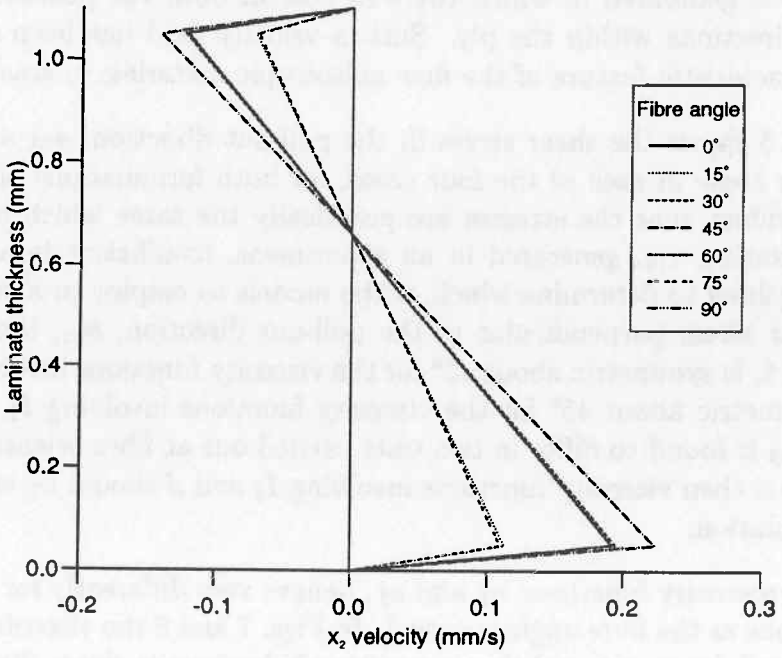

Figure 4: Variable viscosity model: typical velocity distribution in the x_2-direction

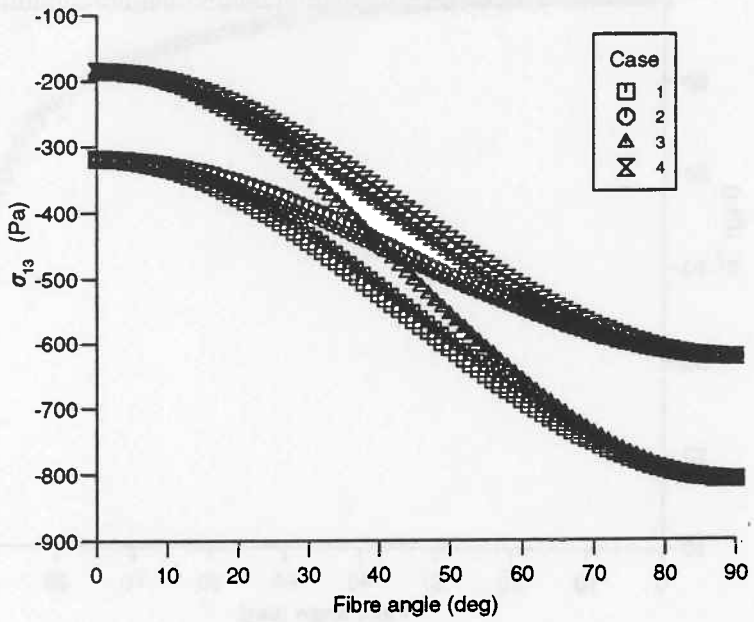

Figure 5: Shear stress σ_{13} as a function of fibre angle. Large (small) symbols represent viscosity functions involving I_1 (I_2 and J)

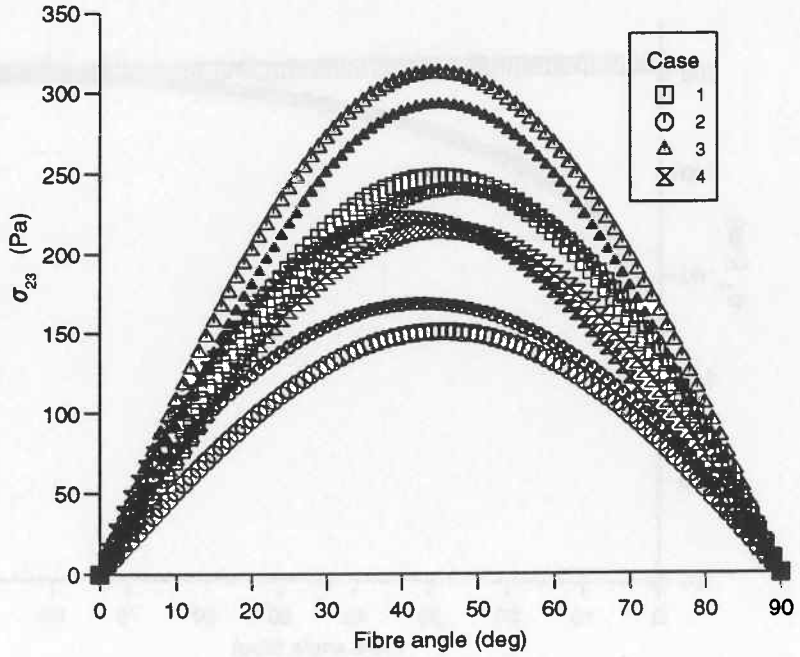

Figure 6: Shear stress σ_{23} as a function of fibre angle. Large (small) symbols represent viscosity functions involving I_1 (I_2 and J)

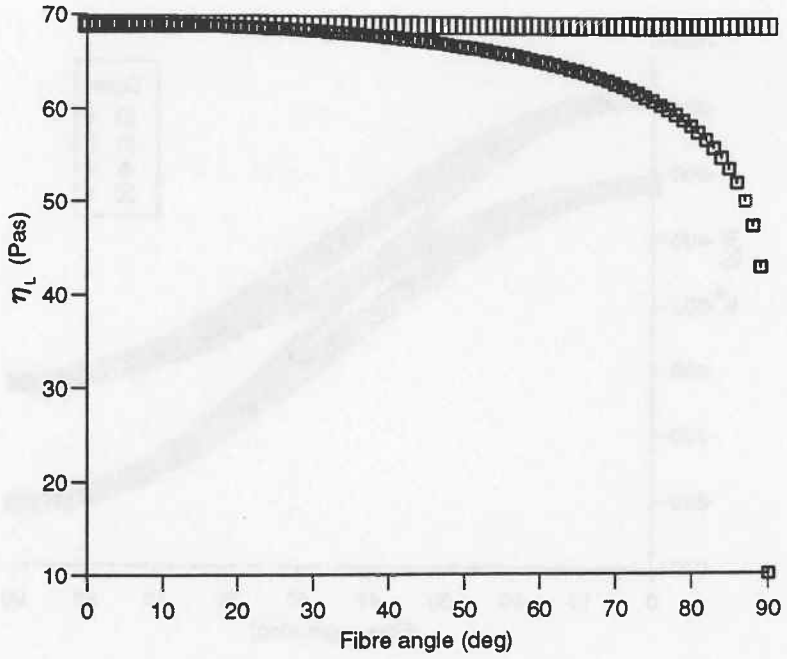

Figure 7: Variation of the longitudinal viscosity function for Case 1. Large (small) symbols represent viscosity functions involving I_1 (I_2 and J)

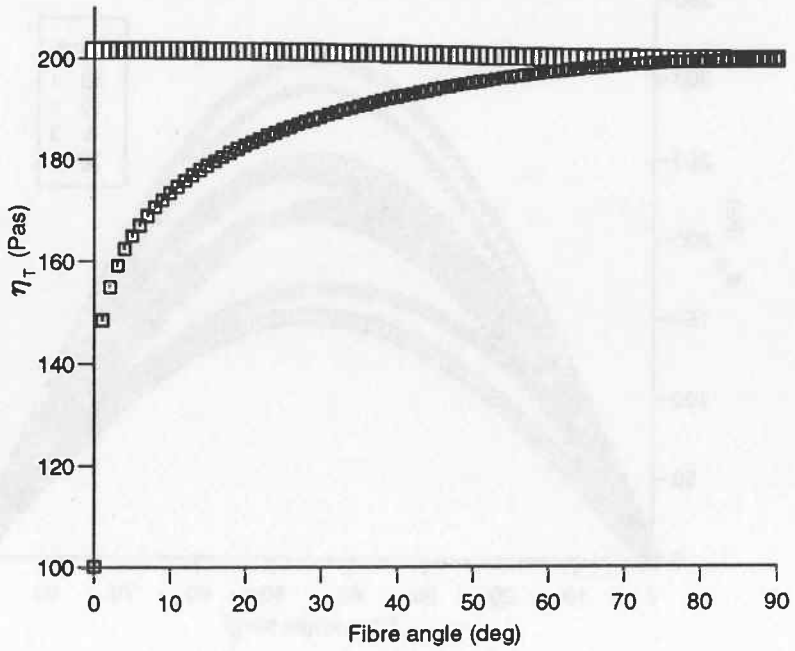

Figure 8: Variation of the transverse viscosity function for Case 1. Large (small) symbols represent viscosity functions involving I_1 (I_2 and J)

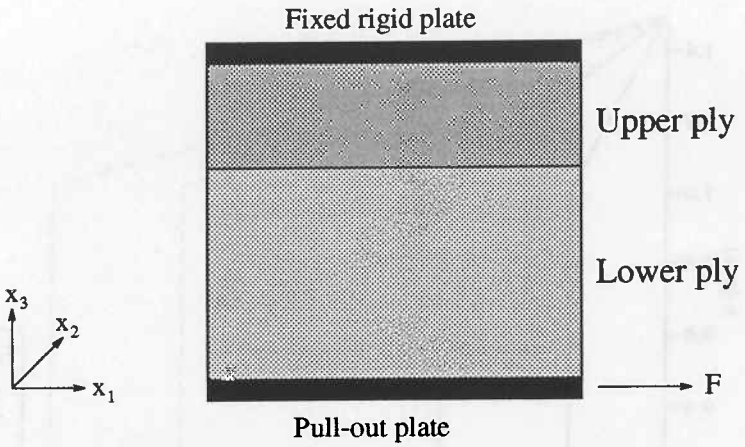

Figure 9: Geometrical configuration for the yield stress model example

of two plies is considered, as shown in Fig. 9. The parameters used in the model of the plies are given in Appendix A. A range of forces were applied to the lower rigid plate, to displace it in the x_1-direction. If the flow in the x_1-direction is considered, below a certain value no significant flow occurs since the stress applied to the material is below the yield stress in both plies. As the force is increased the upper layer yield as shown in Fig. 10. Since, for the parameters chosen, the yield value is greater in the lower layer the fluid in that layer behaves as a solid and displays the characteristic plug flow associated with yield stress materials. As the force on the lower plate is further increased the lower layer yields, as shown in Fig. 11. Further increases in the stress lead to the velocity profiles in Fig. 12 which show that for this example, upon yielding, the lower layer flows more readily than the upper layer. In the x_2-direction, no flow occurs until the higher yield value of the two plies is exceeded. Upon the lower layer yielding the velocity profiles in Fig. 13 are generated.

The response of the model as the fibre angle is changed is shown in Figs. 14–16. The fibres in the two plies are at the same angle in Figs. 14 and 15 which show velocity profiles when just the top ply has yielded and when both plies have yielded respectively. In Fig. 16 the fibres in the two plies are at different angles, in general, and both plies have yielded.

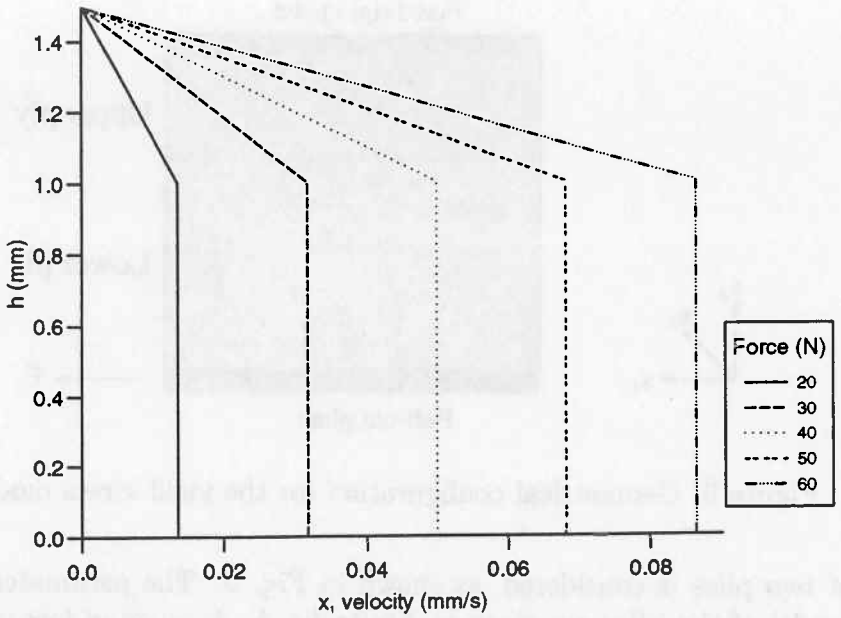

Figure 10: Yield stress model: velocity distribution in the x_1-direction, lower layer unyielded

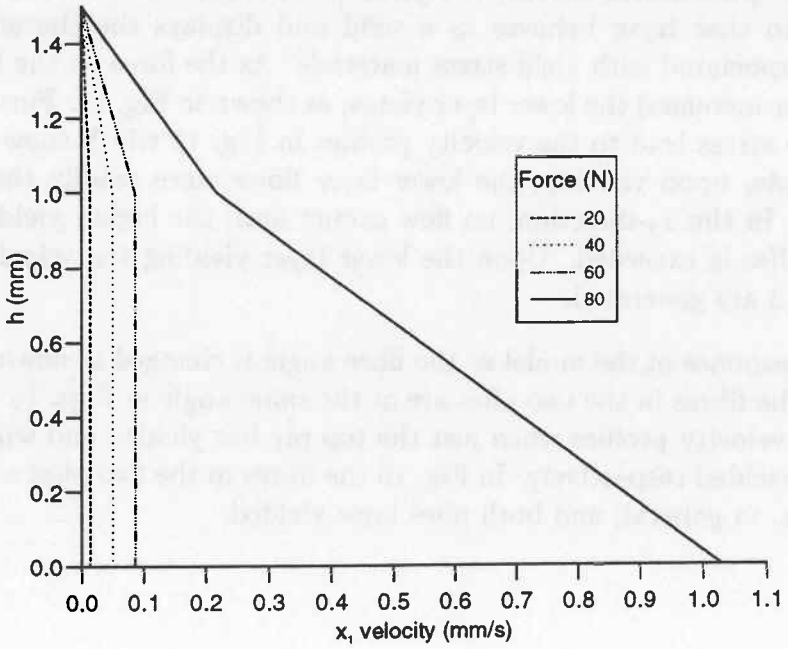

Figure 11: Yield stress model: velocity distribution in the x_1-direction as the lower layer yields

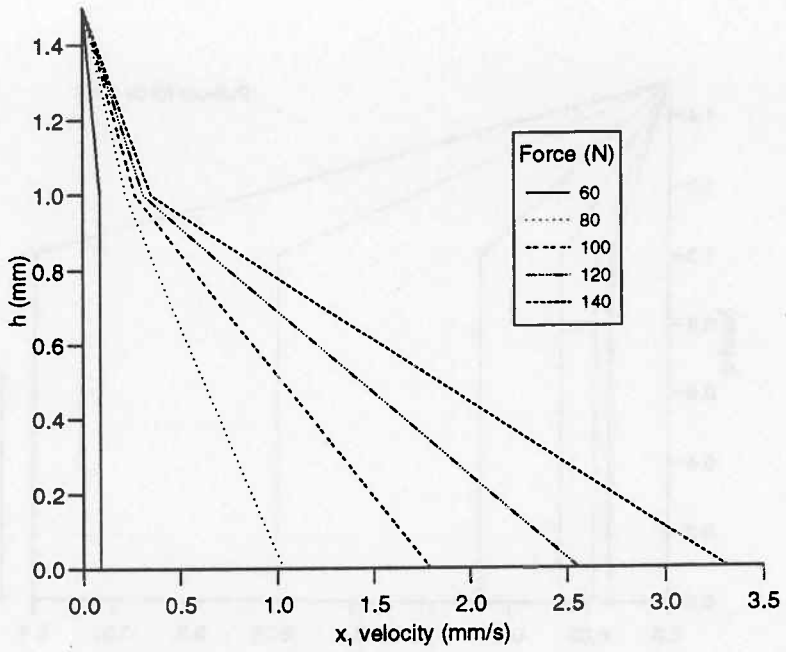

Figure 12: Yield stress model: development of the velocity distribution in the x_1-direction after the lower layer has yielded

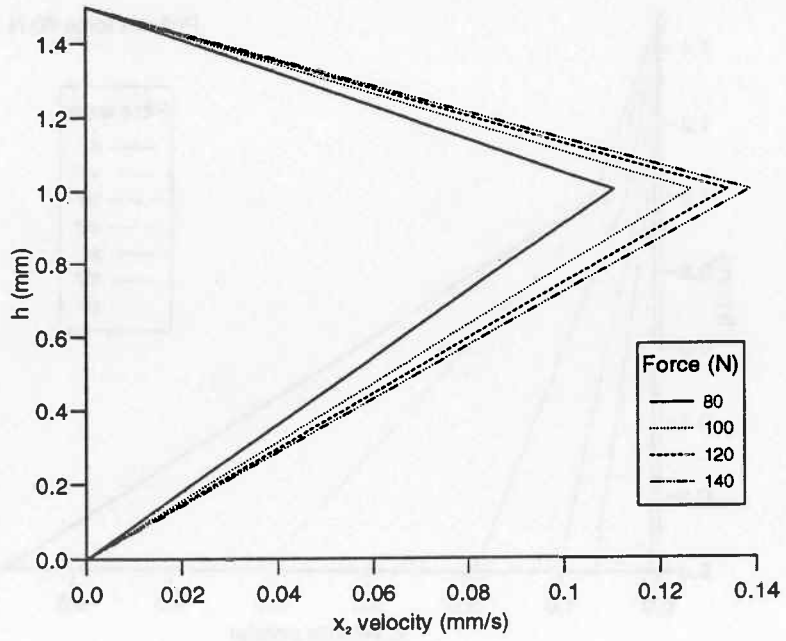

Figure 13: Yield stress model: velocity distribution in the x_2-direction

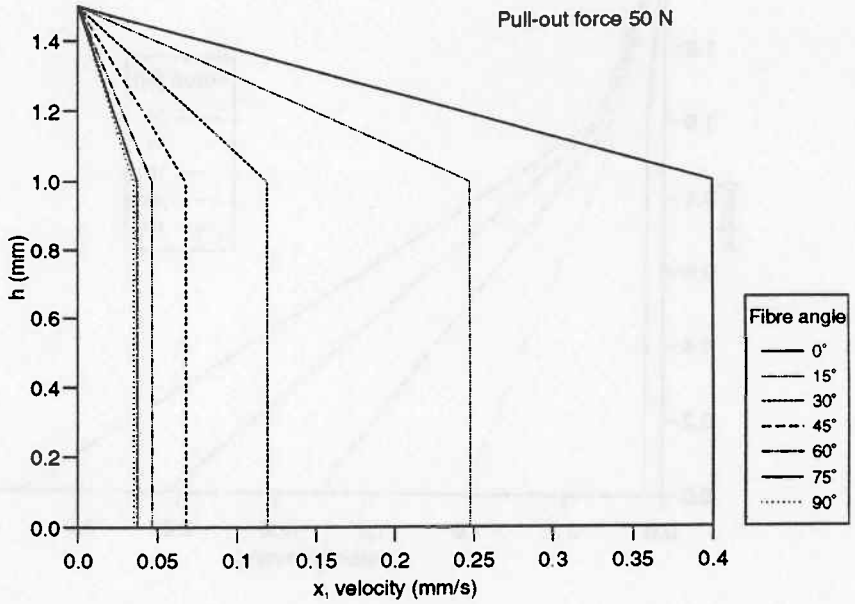

Figure 14: Yield stress model: effect of fibre orientation on velocity in the x_1-direction, fibre angles the same in both plies, lower ply unyielded

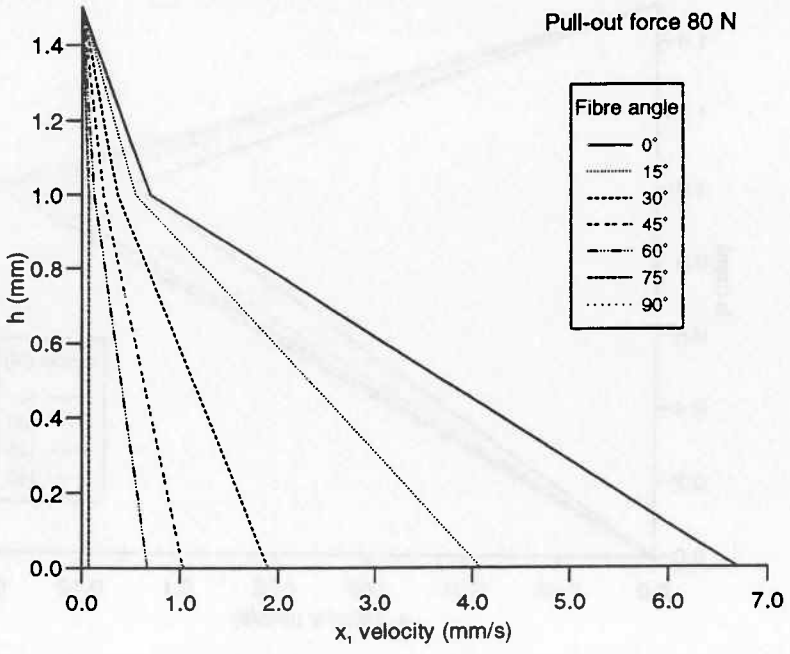

Figure 15: Yield stress model: effect of fibre orientation on velocity in the x_1-direction, fibre angles the same in both plies, both plies yielded

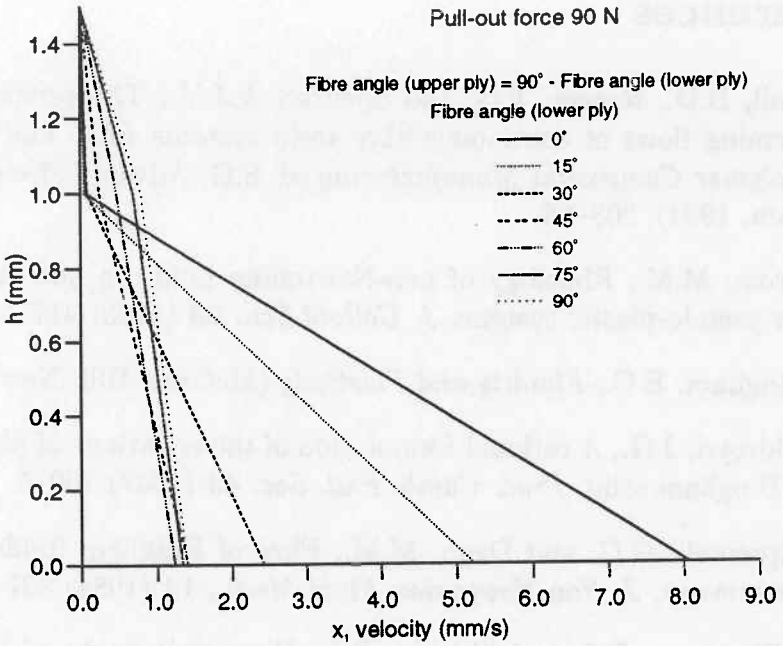

Figure 16: Yield stress model: effect of fibre orientation on velocity in the x_1-direction, fibre angles differ in the two plies, both plies yielded

5 Conclusions

Two anisotropic constitutive relations, particularly suited to the study of continuous fibre-reinforced composites, have been presented. In the first the longitudinal and transverse viscosities are assumed to depend on tensor invariant quantities related to the rate-of-strain tensor and the fibre-orientation vector. In the second an anisotropic yield condition is imposed and upon yielding the material behaves anisotropically. The response of these models in a steady flow, which ultimately reduces to a steady pure shear flow, has been investigated.

For isotropic materials, yield stress models and generalized Newtonian models have been combined in the Herschel-Bulkley model [8] in which the stress and rate-of-strain have a power-law dependence beyond the yield point. A natural extension of the present work would be to combine the two new models to produce an anisotropic equivalent of the Herschel-Bulkley model.

References

[1] Hull, B.D., Rogers, T.G. and Spencer, A.J.M., Theoretical analysis of forming flows of continuous-fibre–resin systems *Flow and Rheology in Polymer Composites Manufacturing* ed. S.G. Advani (Elsevier, Amsterdam, 1994), 203–56

[2] Cross, M.M., Rheology of non-Newtonian fluids: a new flow equation for pseudo-plastic systems *J. Colloid Sci.*, **20** (1965) 417–37

[3] Bingham, E.C., *Fluidity and Plasticity* (McGraw-Hill, New York, 1922)

[4] Oldroyd, J.G., A rational formulation of the equations of plastic flow for a Bingham solid, *Proc. Camb. Phil. Soc.* **43** (1947) 100–5

[5] Lipscomb, G.G. and Denn, M.M., Flow of Bingham fluids in complex geometries, *J. Non-Newtonian Fluid Mech.*, **14** (1984) 337–46

[6] O'Donovan, E.J. and Tanner, R.I., Numerical study of the Bingham squeeze film problem, *J. Non-Newtonian Fluid Mech.*, **15** (1984) 75–83

[7] Goshawk, J.A. and Jones, R.S., The flow of continuous fibre-reinforced composites in steady shear, *Comp. Sci. Technol.*, **56** (1996) 63–74

[8] Herschel, W.V.H. and Blukley, R., Konsistenzmessungen von Gummi-Benzollösungen, *Kolloid Z.*, **39** (1926) 291–300

Appendix A

Parameter values used in the models

Variable viscosity model

Lower resin layer
Thickness 0.05 mm; Viscosity 70 Pas

Upper resin layer
Thickness 0.05 mm; Viscosity 110 Pas

Ply
Thickness 1 mm; η_L^∞ =10 Pa s; η_L^0 =100 Pa s; η_T^∞ =100 Pa s; η_T^0 =800 Pa s

Case	n_L	C_L	n_T	C_T
1	1.3	1024	1.2	0.4
2	1.3	1024	0.6	1.6
3	0.4	0.03	1.2	0.4
4	0.4	0.03	0.6	1.6

Yield stress model

Ply	η_y Pa s	η_L Pa s	η_T Pa s	σ_L Pa	σ_T Pa	h mm
Lower	10^{10}	5	50	50	60	1
Upper	10^{10}	50	500	10	15	0.5

Note, h refers to the thickness of a ply.